

**MINERAL MAPPING IN VALLES MARINERIS, MARS: A NEW APPROACH TO SPECTRAL DEMIXING OF TES DATA.** L.R. Gaddis, M.I. Staid, J.R. Johnson and T.N. Titus, U.S. Geological Survey, Flagstaff, AZ, lgaddis@usgs.gov.

**Introduction:** We applied multiple endmember demixing [1, 2] to Thermal Emission Spectrometer (TES) data to determine the composition of geologic units in the Valles Marineris (VM), Mars. The goal is to map the compositions of VM dark deposits [3] and layered units of the walls and interior deposits [4-6].

**Background:** The Valles Marineris (**Fig. 1**) offer 3-D views into the Martian crust to depths of up to 10 km [7, 8]. The VM are thought to expose the record of geologic history of Mars from early evolution of the crust and possible formation of a megaregolith, through modification by volcanism, possible lacustrine and other hydrologic activity, to tectonic processes that formed and modified the chasmata [9-12]. Determination of the origin of layered deposits in the VM offers insight into geologic history and past climates on Mars and may provide evidence for sites of recent activity that are suitable habitats for life.

**Current Work:** VM geologic units are diverse [13] and are likely to contain minerals (e.g., pyroxenes, plagioclase, olivine) and weathering products (clay minerals) that have diagnostic signatures in the TES 6- to 40-micron wavelength range. In addition to characterizing the layered units in VM, two other deposits are of interest: young, dark materials within the chasmata floor [3], and possible iron oxides at Ceti Mensa in west Candor Chasma [14, 15].

New software in ISIS was used to extract and process the 143-channel TES data ( $10\text{ cm}^{-1}$ ) prior to demixing. TES emissivity data were extracted using the program "vanna" (an ISIS interface to the ASU "vanilla" software) over the VM. These nadir, daytime TES data have surface temperatures between  $250^{\circ}$  to  $350^{\circ}$  K, incidence angles between  $0$  and  $80^{\circ}$ , and emission angles less than  $10^{\circ}$ . To reduce noise, up to 6 detector elements were averaged for each orbit and instrument observation, and average emissivities were reported for each detector footprint. These data were then sorted by surface temperature, and the ISIS "lev2raster" program was used to place TES pixels with warmest data on top.

The spectral deconvolution is a revision of our previous approach [2] and focuses on the use of multiple endmember spectral mixture analysis [MESMA; 1] to remove atmospheric components and to analyze TES data relative to laboratory spectral measurements of common minerals. This method identifies the minimum number of components required to model the spectrum of each pixel in the spectral ranges of 233-

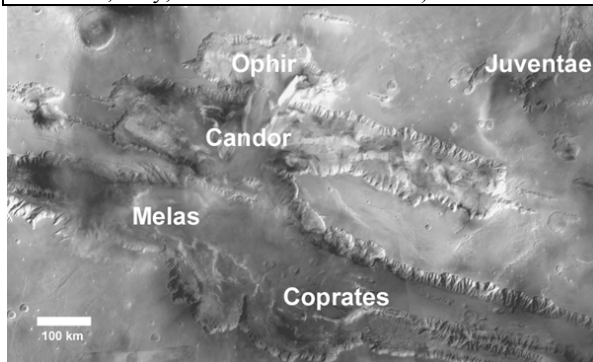
$509\text{ cm}^{-1}$  and  $827\text{-}1304\text{ cm}^{-1}$  (73 TES channels) through comparison to a 46-component library. The current algorithm compares all 3-endmember combinations from the minerals, atmospheric, and blackbody components. The best model with positive endmember (EM) abundances for each spectrum is identified on the basis of the computed RMS error for each combination. Each unused mineral EM is added in turn to the 6 EMs and a new RMS error is calculated. The spectrum that has positive abundance for all components and provides the best improvement is kept as an additional EM. If no additional EM is selected, the previous best solution is kept. This procedure is iterated until up to 12 mineral EMs are selected. The result is an image cube with 46 fraction images for 39 minerals (comparable to that of [16], with red and nanophase hematite, and Pahala ash and JSC-1 Mars palagonitic soils added), 6 atmospheric EMs, and a blackbody, plus RMS and residual error images. Mineral fraction images are then combined into 17 mineral groups and displayed in 3-group combinations [e.g., 15, 16].

**Results:** **Figures 2-6** show the results of applying MESMA to TES data for the Valles Marineris. The RMS error image (**Fig. 2**) shows that error is low ( $<0.005$ ) everywhere, with most error associated with clouds and surface dust on the plateau (e.g., north of east Candor; **Fig. 3**, after [17]). Atmospheric components (**Fig. 4**) show substantial variation, including a correspondence with topography, with clouds prominent at high elevations and higher dust levels in the canyon. Blackbody ( $\sim$ surface dust) is ubiquitous but is especially prominent where the surface dust index is higher (Figure 3). Mineral abundance maps (**Fig. 5**) show basaltic lithologies for much of the VM interior, in the form of high- and low-Ca pyroxenes (up to 24% total) and plagioclase minerals (up to 28%) in layered deposits in the walls and interior, as well as in dark materials at the base of canyon walls. Note that the presence of surface dust in parts of Ophir and east Candor Chasmata appears to decrease the apparent abundance of minerals in these areas. The distribution of gray hematite agrees well with previous results [18], but we see only ( $\sim$ 8%) a small enrichment of red hematite in the possible hydrothermal site in west Candor [14] (**Fig. 6**). Clay minerals and derived surface dust (Pahala ash and JSC-1) components are widely distributed, with derived dust showing a strong correspondence with the calculated surface dust index.

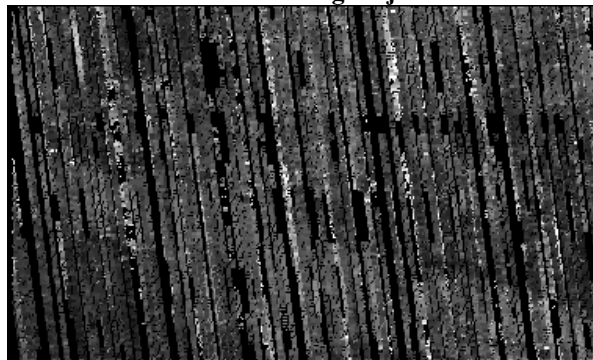
Mapping of pyroxenes and feldspars supports a volcanic origin for much of the dark material in the wall and floor of VM. Olivine may also be associated with some of these young volcanic deposits. These results suggest that we are mapping sites of recent volcanism and aqueous and/or hydrothermal alteration in CVM with the TES data.

**References:** [1] Roberts et al., 1998, Rem. Sens. Env. 65, 267. [2] Staid et al., 2001, Eos Trans. AGU, 82 (47), Fall Meet. Suppl., Abs. P42A-0553. [3] Lucchitta, 1990, Icarus 86, 476. [4] Gaddis and Titus, 2000, LPS XXXI, #1976. [5] Lucchitta, 2001, LPS XXXII, #1359. [6] Malin and Edgett, 2000, Science 290, 1927. [7] Malin et al., 1998, Science 279, 1681. [8] McEwen et al., 1999, Nature 397, 584. [9] Lucchitta et al., 1992, Ch. 14 in Mars, 453. [10] Mustard and Cooper, 1999, 5<sup>th</sup> Int. Conf. Mars, #6168. [11] Treiman, 1999, 5<sup>th</sup> Int. Conf. Mars, #6098. [12] Solomon, 1999, 5<sup>th</sup> Int. Conf. Mars, #6212. [13] Lucchitta, 1999, USGS Map I-2568. [14] Geissler et al., Icarus, 106, 380-391. [15] Gaddis et al., 2002, Eos Trans. AGU, 83 (47), Fall Meet. Suppl., Abs. P62A-0361. [16] Bandfield., 2002, JGR-P 107, 10.1029/2001JE001510. [17] Ruff and Christensen, 2001, 1<sup>st</sup> MER Landing Site Workshop, #9026. [18] Christensen et al., 2001, JGR 106, 23873.

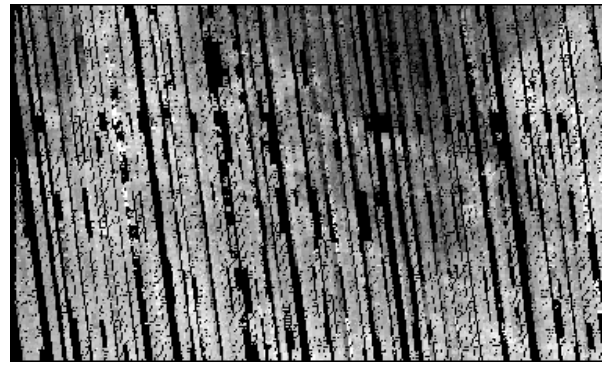
**Figures.** The Valles Marineris, Mars: **1)** MOC WA mosaic; **2)** MESMA results, RMS Error; **3)** Surface Dust Index (after [17]). **4-6)** TES data showing MESMA results for **4)** Atmospheric endmembers, and mineral abundance maps for **5)** Basaltic lithologies (Clinopyroxene, Plagioclase, and Orthopyroxene) and **6)** Soils (Nanophase Red Hematite, Clay, and derived Surface Dust).



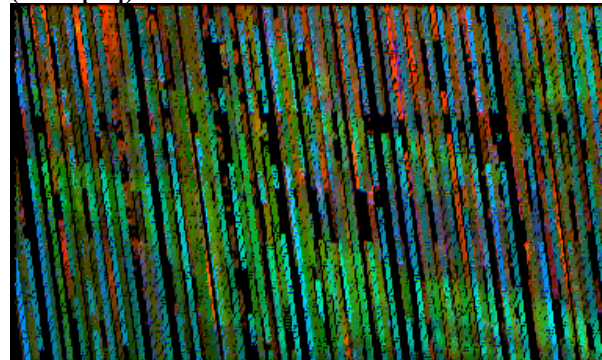
**1. MOC WA mosaic showing major VM chasmata.**



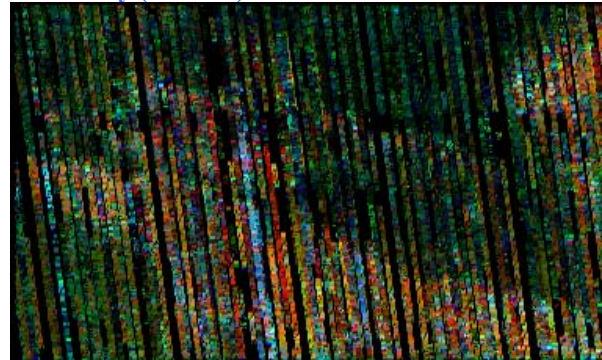
**2. MESMA Results, RMS Error: 0.001 to 0.005.**



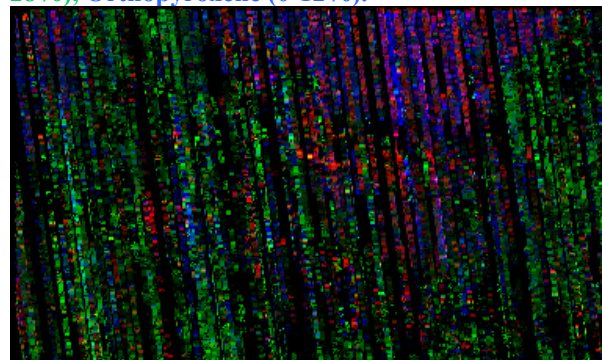
**3. Surface dust index: 0.90 (high dust, dark) to 0.99 (low dust, bright), average emissivity, 1350-1400 wn (after [17]).**



**4. Atmosphere: Clouds (0-100%), Dust (0-80%), Blackbody (0-100%).**



**5. Basalt: Clinopyroxene (0-12%), Plagioclase (0-28%), Orthopyroxene (0-12%).**



**6. Soils: Red Hematite (0-10%), Clay (0-30%), Surface Dust (0-40%).**